

**Adhesion-induced Phase Separation of Biomembranes—Effective Potential
and Simulations**

Jia-Yuan Wu

Department of Physics and Center for Complex Systems,

National Central University,

Chungli, 32054

Taiwan

September, 2005

Abstract

We present theoretical analyses and numerical simulations for the adhesion-induced phase separation of multi-component membranes with two types of ligand-receptor complexes (junctions). We show that after integrating all possible distributions of the junctions, the system can be regarded as a membrane under an effective external potential. Mean field theory and Gaussian approximation are used to analyze the effective membrane potential and we find (i) The height difference of the junctions is the main factor that drives phase separation at sufficiently large junction height difference. (ii) In the two phase region far from the mean-field critical point, because of the higher entropy associated with the softer junctions, phase coexistence occurs when the effective binding energy of the more rigid junctions is higher. (iii) In the two phase region near the mean-field critical point, the shape of the effective potential shows that the phase coexistence occurs when the effective binding energy of softer junctions is higher. The effect of junction density on the critical point is studied by Monte Carlo simulations, and the result shows that phase separation occurs at larger junction height difference as junction density of the system decreases.

Contents

1	Introduction	1
2	The Model	3
2.1	The Hamiltonian	4
2.2	Phase Diagram: Zero Fluctuation	8
2.2.1	Symmetric Case	10
2.2.2	Asymmetric Case	13
2.3	Gaussian Approximation	18
2.4	Summary	22
3	Numerical Simulation	23
3.1	Monte Carlo Simulation	23
3.1.1	Metropolis Algorithm	23
3.1.2	Monte Carlo Steps	24
3.1.3	Snapshots in MC Simulations	24
3.2	The Binder Cumulant and Critical Point	31
3.3	Results and Discussions	31

4	Conclusions	37
A	Elasticity of two fluctuating membranes	42
B	Nondimensionalization of the Hamiltonian	44

Notation

Material parameters

symbol	dimensionless form	physical meaning
κ		bending rigidity
γ	$\frac{\gamma_\alpha a^2}{\kappa}$	surface tension
λ_α	$\frac{\lambda_\alpha a^2}{\kappa}$	elastic constant of type- α junction
h_α	ℓ_α	natural length of type- α junction
$E_{B\alpha}$	$\tilde{E}_{B\alpha}$	binding energy of type- α junction
Φ_α	ϕ_α	density of type- α junction
μ_α	$\tilde{\mu}_\alpha$	chemical potential of type- α junction
a		lattice constant in the $x - y$ plane
h_0		unit length in the z -direction
$k_B T$		energy unit

Defined parameters

$\ell_0 = \frac{\ell_1 + \ell_2}{2}$	the average height of the two junctions
$\Delta_h = \frac{\ell_2 - \ell_1}{2}$	length difference of the two junctions
$\Lambda_\alpha = \frac{\lambda_\alpha a^2}{\kappa}$	dimensionless junction elastic constant
$\Lambda_+ = \Lambda_1 + \Lambda_2$	sum of the junction elastic constant
$\Lambda_- = \Lambda_1 - \Lambda_2$	difference of the junction elastic constant
$\lambda = \frac{\Lambda_-}{\Lambda_+}$	junction flexibility difference
$E_{eff\alpha} = \tilde{E}_{B\alpha} + \tilde{\mu}_\alpha$	effective binding energy
$E_{eff+} = E_{eff1} + E_{eff2}$	sum of the effective binding energy
$E_{eff-} = E_{eff1} - E_{eff2}$	difference of the effective binding energy
$g = \Delta_h^2 \Lambda_+$	junction height difference

Chapter 1

Introduction

Membrane adhesion has been studied theoretically and experimentally [1]-[11]. It plays an important role in many biological processes ranging from embryological development, repair of tissue, immune response [12], to pathology of tumors [13]. In general, the adhesion is mediated by some kinds of lock-and-key molecular complexes (for simplicity, they are called junctions). An example of membrane adhesion is the formation of immunological synapse between a T lymphocyte (T cell) and an antigen-present cell (APC), a key event of the immune response [12]. In this example a highly organized pattern in membrane adhesion region where the TCR/MHC-peptide complexes aggregate in the center with a peripheral ring composed of the LFA-1/ICAM-1 complexes is observed.

Qi et. al. [14] studied the immunological synapse pattern formation with a theoretical model based on a Landau-Ginzburg free energy and a set of coarse-grained reaction-diffusion equations and suggested that the dynamics of immunological synapse pattern formation is a spontaneous self-assembly process. Later, Ray-

chaudhuri et. al. [15] developed an effective membrane model which is derived from the reaction-diffusion equations in [14] and the condition of forming immunological synapse is studied by the mean field, Gaussian, and renormalization group theories.

In [16] Lipowsky et. al. studied membrane adhesion in the presence of one type of junctions and one type of repellers (repulsive molecules) in their Monte Carlo Simulation. The results show that the phase separation depends on the height difference and the concentration of two types of molecules. Later in [17], they considered membrane adhesion in the presence of two different types of junctions which resembles T cell-APC adhesion. Their study indicated that the phase separation is driven by the height difference between two types of junctions, but the formation of target-patterned immunological synapse has to be assisted by the motion of cytoskeleton.

We study the general case of two membranes binding to each other due to the presence of two types of junctions. Similar system has been studied in [18], where Chen considered the effect of junction flexibility difference on phase separation and developed an equilibrium statistical mechanical analysis which provided a phase diagram in mean field level. In this thesis, we re-examine the system studied in [18] with an effective membrane model that is closely related to [15]. Our goal is to provide a complete picture for the phase separation induced by membrane adhesion which includes the effect of junction height difference, junction flexibility difference, and thermally activated membrane height fluctuations. This thesis is organized as follows. Chapter 2 introduces the model and the effective potential approach, meanwhile mean field theory and Gaussian approximation are introduced to study the phase diagrams of the system. Chapter 3 discusses the simulation. Chapter 4 summarizes this thesis.

Chapter 2

The Model

In this chapter, we introduce the Hamiltonian of the system under consideration and derive the effective potential acting on the membrane. Through the analysis of effective potential in the mean-field approach and Gaussian approximation, a lot of the physics of this system are revealed.

The main compositions of biomembranes are amphiphilic lipids with hydrophilic heads and hydrophobic tails. Besides the lipids, there are many kinds of proteins and carbohydrates. For simplicity, in our model we consider membranes containing only lipids, ligands, and receptors. The adhesion between a substrate-supported membrane and a membrane floating in the solvent is induced by the formation of two types of specific ligand-receptor complexes (in the rest of this thesis, we shall refer them as “junctions”). The geometry of the system under consideration is shown schematically in Fig. 2.1. The height of the upper membrane at \mathbf{r} is denoted as $h(\mathbf{r})$, where $\mathbf{r} = (x, y)$ is a two-dimensional planar vector. The junctions which mediate the membrane adhesion are formed by non-covalent adhesion between type- α (α is 1 or 2)

ligands and type- α receptors. The density of type- α junctions at \mathbf{r} is denoted as $\Phi_\alpha(\mathbf{r})$, and the binding energy of a type- α junction is $E_{B\alpha}$. These ligand-receptor bonds are non-covalent bonds composed of several hydrogen or van der Waals- like interactions. Typical binding energy for a ligand-receptor pair is on the order of $10 k_B T$. Our model geometry directly applies to the experimental set up in [12]. In Appendix A, we show that by suitable transformation, the system with two membranes in the solvent is equivalent to the system described above.

2.1 The Hamiltonian

The energy of this system at any instance has several contributions: (i) the curvature elasticity and surface tension of the membrane, (ii) the binding energy of the ligand-receptor pairs, (iii) the deviation of the ligand-receptor pairs from their natural conformation. Therefore the simplest coarse-grained Hamiltonian that includes all the above effects has the following form

$$H = \int d^2r \left\{ \frac{\kappa}{2} [\nabla^2 h(\mathbf{r})]^2 + \frac{\gamma}{2} [\nabla h(\mathbf{r})]^2 + \sum_{\alpha=1}^2 \Phi_\alpha(\mathbf{r}) \frac{\lambda_\alpha}{2} [h(\mathbf{r}) - h_\alpha]^2 - \sum_{\alpha=1}^2 \Phi_\alpha(\mathbf{r}) E_{B\alpha} \right\}. \quad (2.1)$$

Here κ is the bending rigidity of the membrane (typical value of κ is $2-70 \times 10^{-20} \text{ N}\cdot\text{m}$ [19]). γ is the surface tension of the membrane (typical value of γ is $24 \times 10^{-6} \text{ N/m}$ [20]). In this simple model it is assumed that κ and γ are independent of the composition of the membranes, and the direct interactions between the junctions, free ligands, and free receptors are neglected. The nonspecific interactions between the membranes are

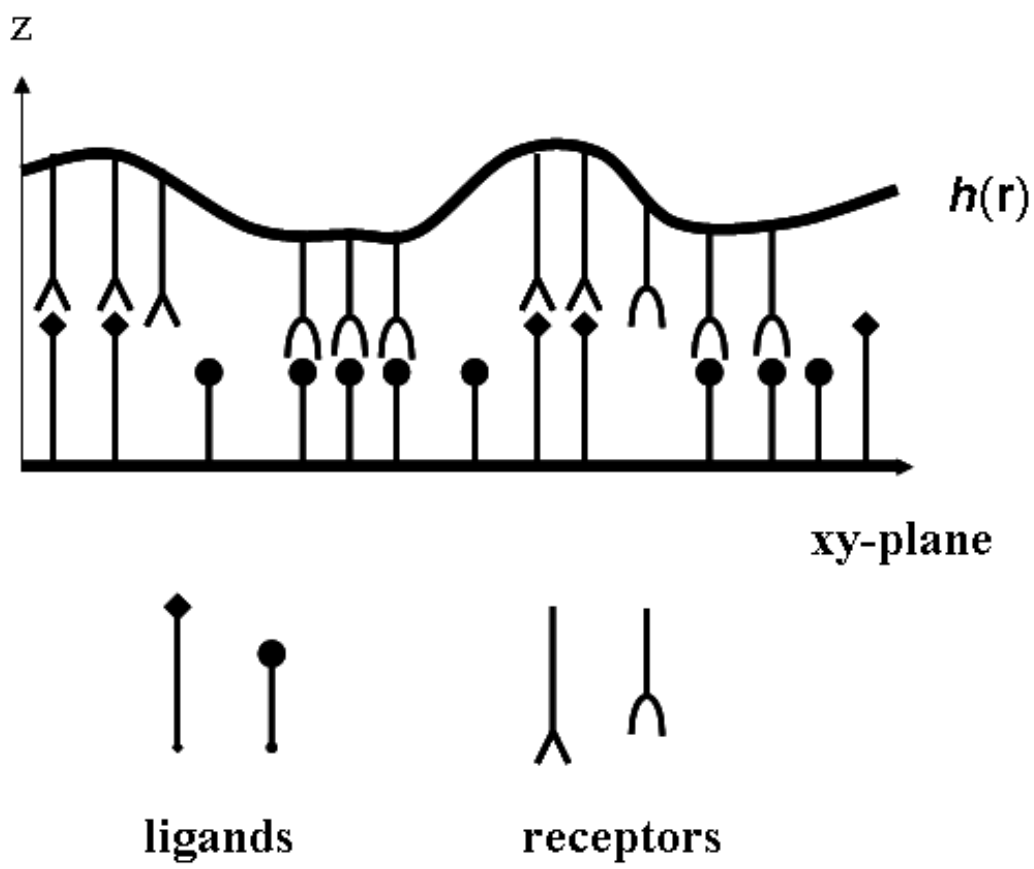


Figure 2.1: The geometry of the system. The system is composed of a substrate-supported membrane in the bottom and an upper membrane floating in the solvent.

Table 2.1: Typical values of material parameters measured for resting cells

parameter	symbol	typical value
bending rigidity	κ	$2 - 70 \times 10^{-20} \text{ N} \cdot \text{m}$ [19]
surface tension	γ	$24 \times 10^{-6} \text{ N/m}$ [20]
junction elastic constant	λ_α	$10^{-5} - 1 \text{ N/m}$ [21]
junction length	h_α	$10 - 30 \text{ nm}$ [21]
junction binding energy	$E_{B\alpha}$	$\sim 10 \text{ } k_B T$
number of or ligands (receptors)		$10^5/\text{cell}$ [21]

also neglected. When a type- α junction is at \mathbf{r} , the interaction energy between the membranes acquires a minimum at $h = h_\alpha$ (the natural height of a type- α junction, typical value 10 - 30 nm [21]), and the coupling term $\sum_{\alpha=1}^2 \Phi_\alpha(\mathbf{r}) \frac{\lambda_\alpha}{2} (h(\mathbf{r}) - h_\alpha)^2$ comes from the Taylor expansion of h around h_α , where λ_α is the flexibility of a type- α junction (typical value of λ_α is $10^{-5} - 1 \text{ N/m}$ [21]). The typical values of the material parameters mentioned above are listed in Table. 2.1. To proceed our discussion, we put the variables $h(\mathbf{r})$ and $\Phi_\alpha(\mathbf{r})$ on a two-dimensional lattice with

lattice constant a . The size of a is chosen to be the smallest length scale beyond which the continuum elastic description of membranes breaks down ($a = 6$ nm [22]). The energy unit is chosen to be $k_B T$, where the unit length in the $x - y$ plane is a and $h_0 = a/\sqrt{\frac{\kappa}{k_B T}}$ in the z direction. That is, $\tilde{E}_{B\alpha} = E_{B\alpha}/k_B T$, $\ell_i = h(\mathbf{r})/h_0$ and $\phi_\alpha(i) = a^2 \Phi_\alpha(\mathbf{r})$. So the non-dimensional form of the Hamiltonian is

$$H_{lat} = \sum_{i=1}^N \left\{ \frac{1}{2} (\Delta_d \ell_i)^2 + \frac{1}{2} \frac{\gamma a^2}{\kappa} (\nabla \ell_i)^2 + \sum_{\alpha=1}^2 \phi_\alpha(i) \left[\frac{1}{2} \frac{\lambda_\alpha a^2}{\kappa} [\ell(i) - \ell_\alpha]^2 - \tilde{E}_{B\alpha} \right] \right\}. \quad (2.2)$$

Where the discretized Laplacian Δ_d in two dimension is given by $\Delta_d \ell_i = \Delta_d \ell_{x,y} = \ell_{x+1,y} + \ell_{x-1,y} + \ell_{x,y+1} + \ell_{x,y-1} - 4\ell_{x,y}$, and the discretized gradient ∇ is $\nabla \ell_i = \nabla \ell_{x,y} = \frac{1}{2}(\ell_{x+1,y} - \ell_{x-1,y})\hat{x} + \frac{1}{2}(\ell_{x,y+1} - \ell_{x,y-1})\hat{y}$. Since the calculation in the canonical ensemble (system with fixed total number of ligands and receptors) is cumbersome. Thus, for simplicity the analysis is carried out in the grand canonical ensemble and we introduce the chemical potential of type- α junction, μ_α ($\mu_\alpha = k_B T \tilde{\mu}_\alpha$). Here we apply the hard-core repulsion between the junctions, consequently each site can be occupied by lipids or one type-1 junction or one type-2 junction. Therefore, the partition function of the system can be written as

$$Z = \int \mathcal{D}[\ell] e^{-H_{el}[\ell]} \prod_{i=1}^N \left[1 + e^{E_{eff1} - \frac{1}{2} \frac{\lambda_1 a^2}{\kappa} (\ell_i - \ell_1)^2} + e^{E_{eff2} - \frac{1}{2} \frac{\lambda_2 a^2}{\kappa} (\ell_i - \ell_2)^2} \right] \quad (2.3)$$

$$= \int \mathcal{D}[\ell] e^{-(H_{el} + U_{eff})}, \quad (2.4)$$

where $E_{eff\alpha} \equiv \tilde{E}_{B\alpha} + \tilde{\mu}_\alpha$ is the effective binding energy which represents the combinations of binding energy of ligand-receptor pairs and entropy lost of free ligands and

free receptors and

$$H_{el} = \sum_{i=1}^N \left[\frac{1}{2} (\Delta_d \ell_i)^2 + \frac{1}{2} \frac{\gamma a^2}{\kappa} (\nabla \ell_i)^2 \right] \quad (2.5)$$

is the elastic energy of the membrane and

$$U_{eff} = - \sum_{i=1}^N \ln \left[1 + \sum_{\alpha=1}^2 e^{E_{eff\alpha} - \frac{1}{2} \frac{\lambda_{\alpha} a^2}{\kappa} (\ell_i - \ell_{\alpha})^2} \right] \equiv \sum_{i=1}^N V_{eff}(i) \quad (2.6)$$

is the effective potential acting on the membrane by summing over all possible distributions of junctions. $V_{eff}(i)$ is the effective potential at site i . The total number of type- α junctions N_{α} in the system can be expressed as the derivative of the Grand potential with respect to the chemical potential.

$$G = -k_B T \ln Z, \quad N_{\alpha} = - \frac{\partial G}{\partial \mu_{\alpha}} = \sum_i \left\langle \frac{e^{E_{eff\alpha} - \frac{1}{2} \frac{\lambda_{\alpha} a^2}{\kappa} (\ell_i - \ell_{\alpha})^2}}{1 + \sum_{\beta} e^{E_{eff\beta} - \frac{1}{2} \frac{\lambda_{\beta} a^2}{\kappa} (\ell_i - \ell_{\beta})^2}} \right\rangle. \quad (2.7)$$

Since typical experiments (either living cells or artificial membranes) are carried out for systems with fixed total number of ligands and receptors. At the end of our analysis we connect $E_{eff\alpha}$ to the corresponding junction binding energies and densities of ligands and receptors in this system, and compare these values with typical biological systems .

2.2 Phase Diagram: Zero Fluctuation

As has been shown in the previous section, the equilibrium membrane height conformation of the system is the same as that of a membrane with effective Hamiltonian

$$\begin{aligned} H_{eff} &= H_{el} + U_{eff} \\ &= \sum_{i=1}^N \left[\frac{1}{2} (\Delta_d \ell_i)^2 + \frac{1}{2} \frac{\gamma a^2}{\kappa} (\nabla \ell_i)^2 - \ln \left(1 + \sum_{\alpha=1}^2 e^{E_{eff\alpha} - \frac{1}{2} \frac{\lambda_{\alpha} a^2}{\kappa} (\ell_i - \ell_{\alpha})^2} \right) \right]. \end{aligned} \quad (2.8)$$

Table 2.2: Dimensionless parameters introduced in Sec. 2.2

$\ell_0 = \frac{\ell_1 + \ell_2}{2}$
$\Delta_h = \frac{\ell_2 - \ell_1}{2}$
$\Lambda_\alpha = \frac{\lambda_\alpha a^2}{\kappa}$
$\Lambda_+ = \Lambda_1 + \Lambda_2, \Lambda_- = \Lambda_1 - \Lambda_2$
$\lambda = \frac{\Lambda_-}{\Lambda_+}$
$E_{eff+} = E_{eff1} + E_{eff2}, E_{eff-} = E_{eff1} - E_{eff2}$
$g = \Delta_h^2 \Lambda_+$

For convenience, several dimensionless parameters are defined in Table. 2.2. Substitute these parameters into Eq. (2.6), $V_{eff}(i)$ can be expressed as a function of

$$\frac{\ell_i - \ell_0}{\Delta_h} \equiv z,$$

$$V_{eff}(i) = -\ln \left[1 + e^{\frac{E_{eff+} - g/2}{2}} A(z) \right], \quad (2.9)$$

where

$$A(z) = e^{\frac{E_{eff-} - g\lambda/2}{2} - g\frac{1+\lambda}{4}[(z+1)^2 - 1]} + e^{-\frac{E_{eff-} - g\lambda/2}{2} - g\frac{1-\lambda}{4}[(z-1)^2 - 1]}. \quad (2.10)$$

The equilibrium membrane height is determined by minimizing $V_{eff}(i)$ with respect to z , i.e.,

$$\frac{dV_{eff}(i)}{dz} = -\frac{e^{\frac{E_{eff+}-g/2}{2}}}{1 + e^{\frac{E_{eff+}-g/2}{2}}A(z)} \frac{dA(z)}{dz} = 0. \quad (2.11)$$

From Eq. (2.11), phase separation occurs when $\frac{dV_{eff}(i)}{dz} = 0$ has three roots (one maximum and two degenerate minimums). Evidently, the value of z that minimizes $V_{eff}(i)$ is independent of E_{eff+} . Therefore, the phase boundary is also independent of E_{eff+} , and only depends on λ , g , and E_{eff-} . However, it will become clear in the next section that this only holds in the mean field theory.

2.2.1 Symmetric Case

In the symmetric case ($\lambda = 0$, i.e., both types of junctions have the same flexibility), the effective potential becomes

$$V_{eff}(i) = -\ln \left[1 + e^{\frac{E_{eff+}-g/2}{2}} \left(e^{\frac{E_{eff-}-g/4}{2}[(z+1)^2-1]} + e^{-\frac{E_{eff-}-g/4}{2}[(z-1)^2-1]} \right) \right]. \quad (2.12)$$

In this case, the minimum of $V_{eff}(i)$ depends on g and E_{eff-} . Since when $E_{eff-} = 0$,

$$A(z) = e^{-\frac{g}{4}[(z+1)^2-1]} + e^{-\frac{g}{4}[(z-1)^2-1]} \quad (2.13)$$

is an even function of z . Phase separation occurs at sufficiently large g , and there are three solutions for $\frac{dA(z)}{dz} = 0$. For small g , there is only a triple root at $z = 0$ which corresponds to $\ell_0 = \frac{1}{2}(\ell_1 + \ell_2)$. And we find that the critical point is located at $(E_{eff-} = 0, g = 2)$. The shape of $V_{eff}(i)$ for two typical cases when phase separation occurs are shown in Fig. 2.2. The parameters for both lines are $\Lambda_1 = \Lambda_2 = 0.2$, $E_{eff1} = E_{eff2} = 1$, $\ell_1 = 15$, for solid line $\ell_2 = 30$ ($g = 22.5$), for dashed line $\ell_2 = 22$

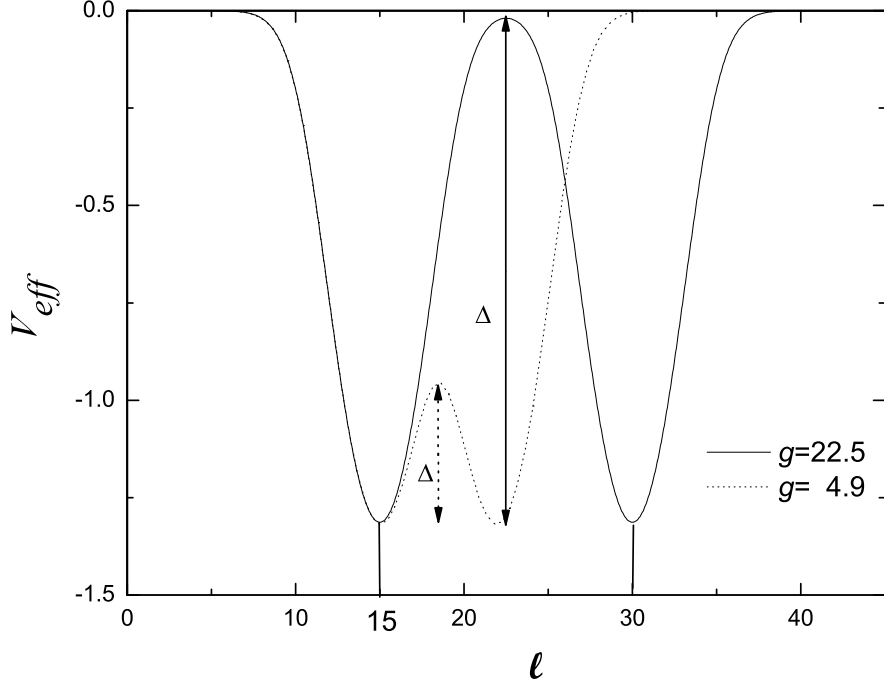


Figure 2.2: The shape of $V_{eff}(i)$ (effective potential) as a function of ℓ for two typical cases when phase separation occurs. The parameters for both lines are $\Lambda_1 = \Lambda_2 = 0.2$, $E_{eff1} = E_{eff2} = 1$, $\ell_1 = 15$, for solid line $\ell_2 = 30$ ($g = 22.5$), for dashed line $\ell_2 = 22$ ($g = 4.9$). The barrier height between the two minimums of $V_{eff}(i)$ is denoted as Δ which is non-zero when phase separation occurs. The minimums are near ℓ_1 and ℓ_2 , the maximum is near $\ell_0 = (\ell_1 + \ell_2)/2$. It also shows that Δ becomes smaller when $\ell_2 - \ell_1$ decreases.

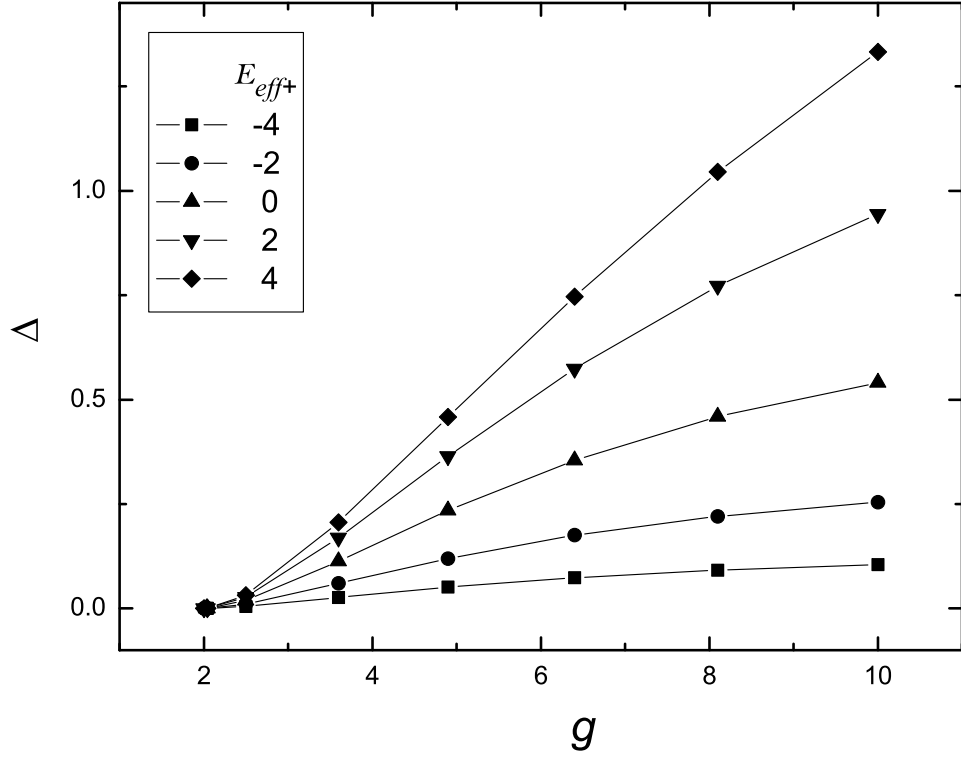


Figure 2.3: The $\Delta - g$ diagram of symmetric case. For different E_{eff+} (by setting $E_{eff1} = E_{eff2}$), the location of the critical point is $g = 2$ which is independent of E_{eff+} . And Δ decreases as E_{eff+} decreases.

($g = 4.9$). The barrier height between the two minimums of $V_{eff}(i)$ is denoted as Δ which is non-zero when phase separation occurs and becomes smaller when $\ell_2 - \ell_1$ decreases. Numerical calculation leads to the critical point locates at ($E_{eff-} = 0$, $g = 2$). This result agrees what we obtain previously. Furthermore, Fig. 2.3 shows that for different E_{eff+} (by setting $E_{eff1} = E_{eff2}$), the critical value of g is always 2. It confirms that the critical point in the mean field theory is independent of E_{eff+} . And we find that the values of Δ decrease as E_{eff+} decreases. That is, the depth of the potential minimums becomes shallower for smaller effective binding energy. From the above analysis, we know that the phase separation is driven by junction height difference, and this separation only occurs when g is sufficiently large.

2.2.2 Asymmetric Case

Let us consider the more general case $\lambda \neq 0$, i.e., different types of junctions have different flexibilities. In this case, the symmetry in $\lambda = 0$ case no longer exists. Therefore we expect that the phase coexistence curve is no longer located at $E_{eff-} = 0$ line. An analytical expression of the phase coexistence curve can be found for $|\lambda| \ll 1$ by expanding $\frac{dA(z)}{dz}$ around $\lambda = 0$, where $A(z)$ is taken from Eq. (2.10). The critical point for $\lambda \neq 0$ locates at the triple root of $dA(z)/dz = 0$. A straightforward calculation similar to [18] leads to the position of the critical points for small λ ,

$$g = 2\left(1 - \frac{\lambda^2}{4}\right) + \mathcal{O}(\lambda^4), \quad (2.14)$$

$$E_{eff-} = -\lambda + \mathcal{O}(\lambda^3). \quad (2.15)$$

The critical value of g decreases as the junction flexibility difference increases, and E_{eff-} , λ have opposite sign. We present the phase coexistence curve in two different ways. Fig. 2.4 shows phase boundaries for $E_{eff+} = 2$, $\Lambda_+ = 0.3$, and $\lambda = 1/3$ (square), $4/15$ (circle), and $1/6$ (triangle). Fig. 2.5 shows phase boundaries for $E_{eff+} = 2$, $\Lambda_1 = 0.2$, $\Lambda_+ = 0.3$, and $\lambda = 1/3$ (square), $1/7$ (triangleleft), and $1/15$ (triangleright). Both figures indicate that near the critical point, phase coexistence curves shift away from $E_{eff-} = 0$ line due to the junction flexibility difference. Furthermore, at large g , the phase boundaries are close to $E_{eff-} = 0$ line. To understand the physics of the phase boundary in small g region, we plot $V_{eff}(i)$ as a function of ℓ in Fig. 2.6 with $E_{eff1} = E_{eff2} = 1$, $\Lambda_1 = 0.2$, $\Lambda_2 = 0.1$ ($\lambda = 1/3$), $\ell_1 = 15$, and $\ell_2 = 22$ ($g = 3.657$). The solid curve is V_{eff} , dotted curve for $-\ln \left[1 + e^{E_{eff1} - \frac{\Lambda_1}{2}(\ell - \ell_1)^2} \right]$ which is the effective membrane potential without the contribution of type-2 junction, and dashed curve for $-\ln \left[1 + e^{E_{eff2} - \frac{\Lambda_2}{2}(\ell - \ell_2)^2} \right]$ which is the effective membrane potential without the contribution of type-1 junction. At small g , the phase boundary shifts away from $E_{eff-} = 0$ line because the minimum energy of the more rigid junctions is “lowered” by the softer junctions. Thus, in the region where the height difference is not very large, phase coexistence occurs when the effective binding energy of the more rigid junctions is smaller (the effective binding energy of the softer junctions is larger).

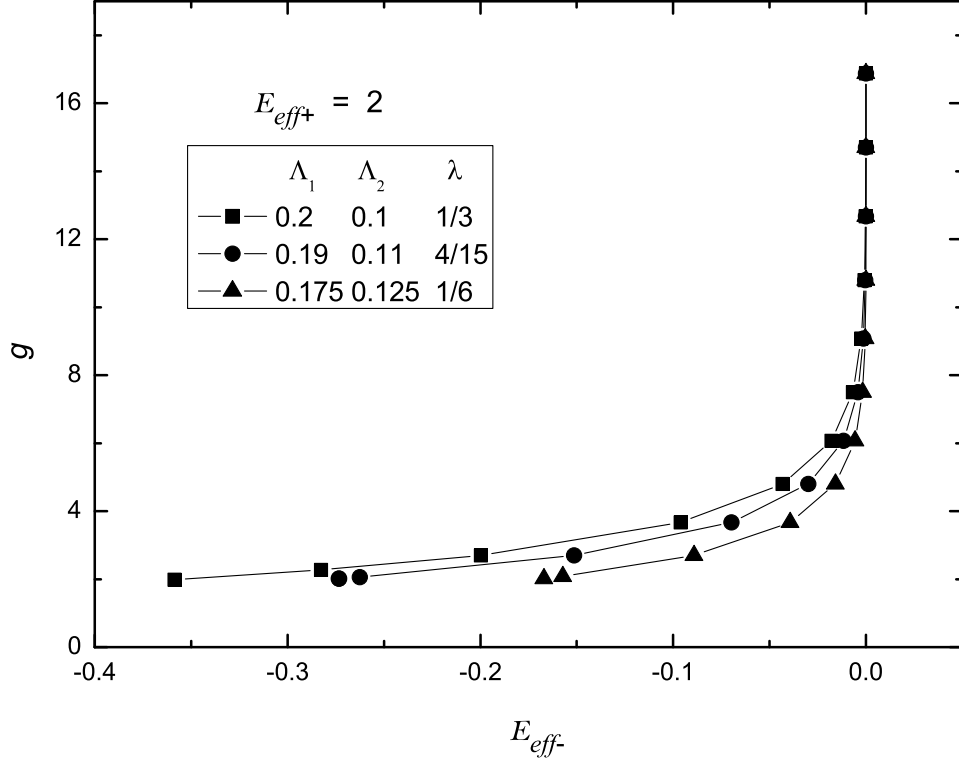


Figure 2.4: Mean field phase boundaries for $E_{eff+} = 2$, $\Lambda_+ = 0.3$, and $\lambda = 1/3$ (square), $4/15$ (circle), and $1/6$ (triangle). We find that near the critical point, phase coexistence curves shift away from $E_{eff-} = 0$ line due to the junction flexibility difference. Furthermore, at large g , the phase boundaries are close to $E_{eff-} = 0$ line.

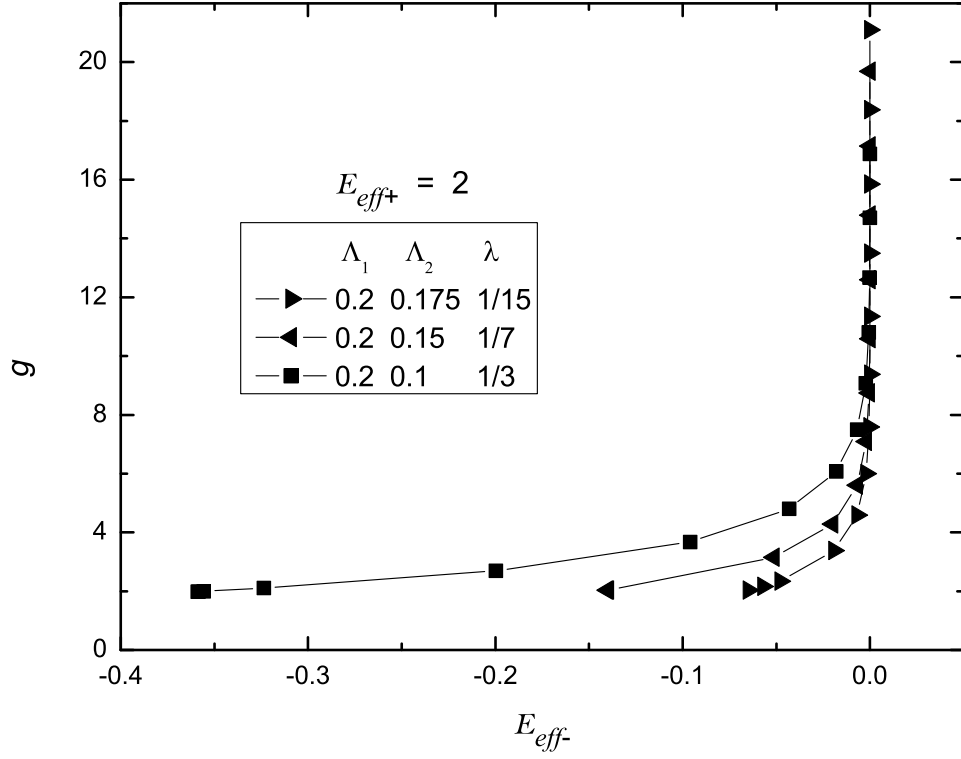


Figure 2.5: Mean field phase boundaries for $E_{eff+} = 2$, $\Lambda_1 = 0.2$, $\Lambda_+ = 0.3$, and $\lambda = 1/3$ (square), $1/7$ (triangleleft), and $1/15$ (triangleright). We find that near the critical point, phase coexistence curves shift away from $E_{eff-} = 0$ line due to the junction flexibility difference. Furthermore, at large g , the phase boundaries are close to $E_{eff-} = 0$ line.

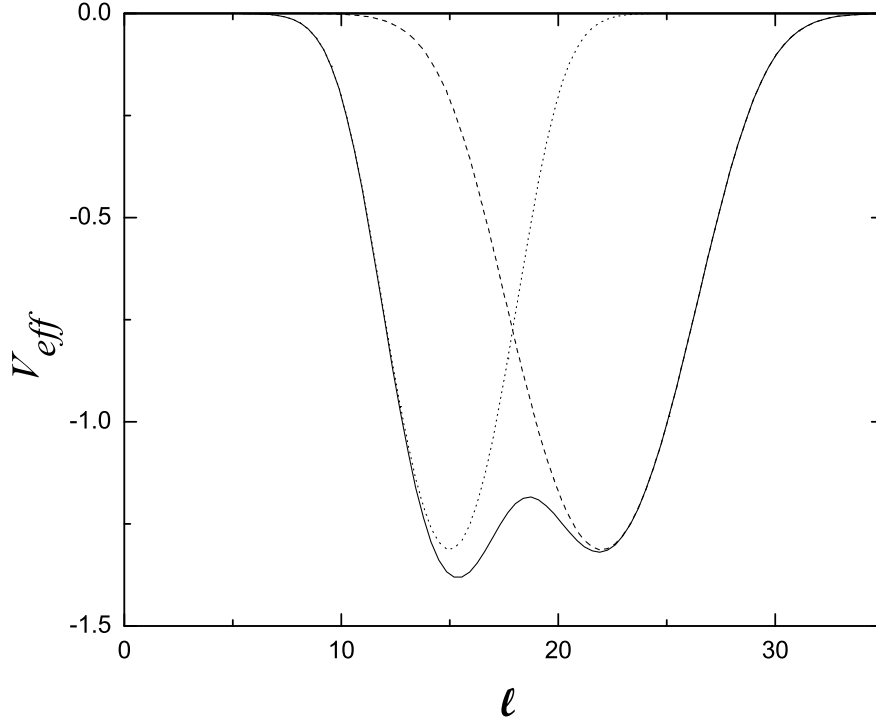


Figure 2.6: Effective potential as a function of ℓ in the small g region with $E_{eff1} = E_{eff2} = 1$, $\Lambda_1 = 0.2$, $\Lambda_2 = 0.1$ ($\lambda = 1/3$), $\ell_1 = 15$, and $\ell_2 = 22$ ($g = 3.657$). The solid curve is V_{eff} , dotted curve for $-\ln \left[1 + e^{E_{eff1} - \frac{\Lambda_1}{2}(\ell - \ell_1)^2} \right]$ which is the effective membrane potential without the contribution of type-2 junction, and dashed curve for $-\ln \left[1 + e^{E_{eff2} - \frac{\Lambda_2}{2}(\ell - \ell_2)^2} \right]$ which is the effective membrane potential without the contribution of type-1 junction. The softer junctions are longer than the more rigid junctions. The minimum energy of the more rigid junctions is “lowered” by the the softer junctions.

2.3 Gaussian Approximation

In the mean field analysis, we assume that the membrane height is chosen to minimize V_{eff} , phase coexistence occurs when there are two degenerate minimums, and the critical point is located at where barrier height between the degenerate minimums vanishes. In this section, we introduce Gaussian approximation to study the fluctuation effects on phase boundaries. Since in equilibrium, the membrane height fluctuates around the potential minimums, the free energy for a membrane with average height at $\ell_{\min\alpha}$ (a minimum of V_{eff}) in the Gaussian approximation is calculated by expanding V_{eff} around $\ell_{\min\alpha}$, i.e.,

$$\frac{F_\alpha}{k_B T} = -\ln \int \mathcal{D}[\ell] e^{-[H_{el} + \int d^2 r V_{eff}(\ell_{\min\alpha}) + \frac{1}{2} V_{eff}''(\ell_{\min\alpha})(\ell - \ell_{\min\alpha})^2]}. \quad (2.16)$$

Integrating out these Gaussian fluctuations, the free energy of α 'th minimum per unit area is

$$\frac{F_\alpha^*}{k_B T} = V_{eff}(\ell_{\min\alpha}) - \frac{1}{4\pi} \int_0^{(2\pi)^2} dq \ln \sqrt{\frac{2\pi}{q^2 + \Lambda q + V_{eff}''(\ell_{\min\alpha})}} + \text{const.} \quad (2.17)$$

After comparing the free energy per unit area of the two minimums of V_{eff} , we plot the phase coexistence curves for several choices of parameters in Fig. 2.7 and Fig. 2.8. In large g region, because the softer junctions can be stretched or compressed easier than the more rigid junctions and have higher entropy, comparing to mean field theory predictions, phase coexistence curve moves toward to higher E_{eff1} (E_{eff2}) when $\lambda > 0$ ($\lambda < 0$). In Fig. 2.7, phase boundaries for several systems with $E_{eff+} = 2$, $\Lambda_+ = 0.3$, and $\lambda = 2/3$ (circle), $1/3$ (square), and $1/6$ (triangle) are shown. In large g region, because the softer the junctions are, the higher the entropy they have. Thus, the phase

boundary shift is more significant for systems with larger junction flexibility difference. Fig. 2.8 shows the phase boundaries for systems with $\lambda = 1/3$, $E_{eff+} = 2$, $\Lambda_+ = 0.3$, and $E_{eff+} = -4$ (lozenge), -2 (circle), 2 (triangledown), and 10 (triangleleft). In the large g region, the phase coexistence curves are located farther from the $E_{eff-} = 0$ line (the phase boundary predicted by the mean field theory) for systems with smaller E_{eff+} . It is because the entropic effect of the softer junctions is smaller when the total junction density is higher (i.e., E_{eff+} is larger). Fig. 2.7 and 2.8 also indicate that in small g region, because the location of critical points are not altered in the Gaussian theory, therefore the phase boundary goes to the mean field critical point as g decreases.

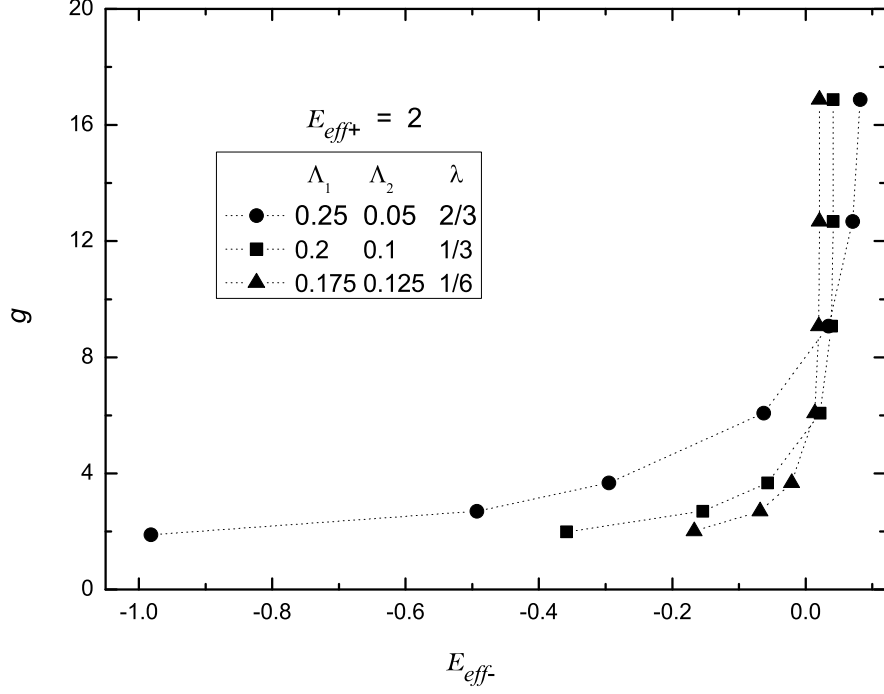


Figure 2.7: Phase boundaries in the Gaussian theory for $E_{eff+} = 2$, $\Lambda_+ = 0.3$, and $\lambda = 2/3$ (circle), $1/3$ (square), and $1/6$ (triangle). Because the softer the junctions are, the higher the entropy they have, comparing to the more rigid junctions. The phase boundaries in the large g region shift away from $E_{eff-} = 0$ line (mean field phase boundary), and the shift is more significant as $|\lambda|$ increases. The critical points in the figure are taken from the result of the mean field theory, because the location of critical points are not altered in Gaussian theory.

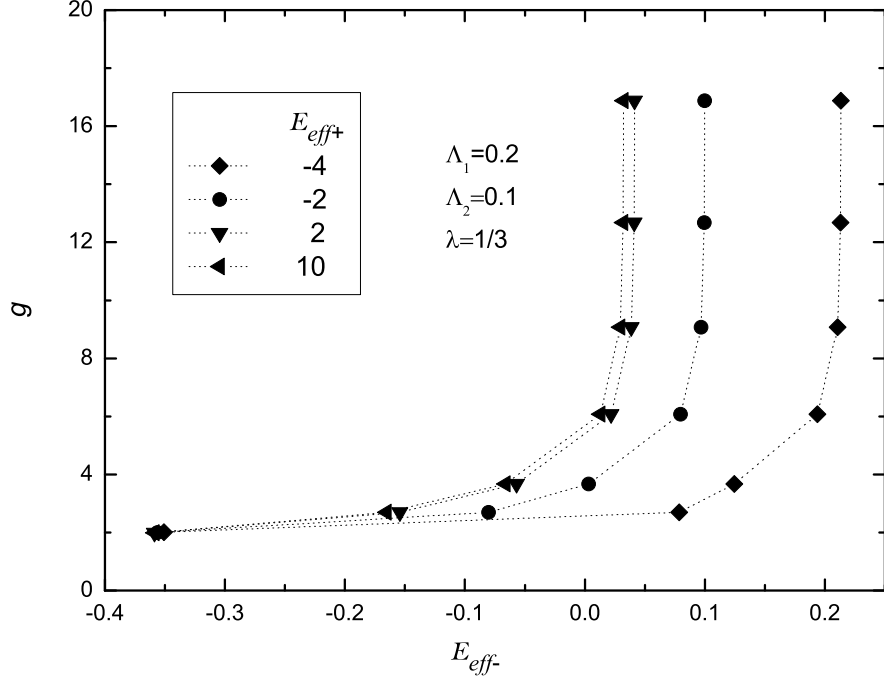


Figure 2.8: Phase boundaries in the Gaussian theory for $\lambda = 1/3$, $E_{eff+} = 2$, $\Lambda_+ = 0.3$, and $E_{eff+} = -4$ (lozenge), -2 (circle), 2 (triangledown), and 10 (triangleleft). The phase boundaries shift away from $E_{eff-} = 0$ line (mean field phase boundary), and the shift is more significant as E_{eff+} decreases. It is because the entropic effect of the softer junctions is smaller when the total junction density is higher (i.e., E_{eff+} is larger). The critical points in the figure are taken from the result of the mean field theory, because the location of critical points are not altered in Gaussian theory.

2.4 Summary

In the mean field analysis, the critical point and phase coexistence curve is independent of the value of E_{eff+} . For symmetric case ($\lambda = 0$), the critical point is located at ($E_{eff-} = 0$, $g = 2$). The phase coexistence curve lies on the $E_{eff-} = 0$ line starting from $g = 2$. In this case, the phase separation is driven by the height difference of the junctions. For asymmetric case ($\lambda \neq 0$), the critical value of g decreases as the junction flexibility difference increases, and the phase boundaries shift away from the $E_{eff-} = 0$ line in smaller junction height difference region due to the minimum of the more rigid junction is “lowered” by the softer junction. In large junction height difference region, the phase boundaries are close to the $E_{eff-} = 0$ line.

In the Gaussian theory, we find that because the state associated with membrane height closer to the natural length of the softer junctions has higher entropy, as a result, comparing to the mean field predictions, in large g region the phase coexistence curves in the Gaussian theory move toward higher E_{eff1} (E_{eff2}) when $\lambda > 0$ ($\lambda < 0$). The phase boundaries shift is more significant when the junction flexibility difference ($|\lambda|$) increases or the total junction density (E_{eff+}) decreases. In small g region, because the location of critical points are not altered in Gaussian theory, thus the phase boundary goes to the mean-field critical point as g decreases.

Chapter 3

Numerical Simulation

3.1 Monte Carlo Simulation

Monte Carlo simulation is a general name for simulations which use random sequences.

It is a way to perform statistical sampling experiments on a computer. It is named after the casino city “Monte Carlo” in the Monaco principality.

3.1.1 Metropolis Algorithm

Metropolis algorithm is applied to our simulations. In the algorithm, if the system is at state i at some instance, first one randomly chooses another state j as the possible new state of the system. Let P_i and P_j be the equilibrium probability for state i and j to occur at temperature T . The energy difference between state i and state j is $\Delta H \equiv E_j - E_i$. If $\Delta H < 0$, then the system changes its state to state j . If $\Delta H > 0$,

then the computer generates a random number $\mathcal{R} \in [0, 1]$. If

$$\mathcal{R} < \mathcal{S} \equiv \frac{P_j}{P_i} = e^{-\Delta H}, \quad (3.1)$$

then the system changes its state to state j , otherwise the system keeps at state i . It can be proved that in the long time limit the simulation generates a series of states that obey Boltzmann distribution [23].

3.1.2 Monte Carlo Steps

In our simulations, the energy of the system depends on the conformation of the membrane. In each MC step, we repeat the following procedure $N = L^2$ times. First, randomly choose a site ($i=(x, y)$). The trial conformation of the membrane is the same as the current state except $\ell_{x,y} \rightarrow \ell'_{x,y} \equiv \ell_{x,y} + \Delta\ell$, where $-5 < \Delta\ell < 5$. This choice corresponds to a height change of maximum size ~ 5 nm. If $\Delta H < 0$, $\ell_{x,y}$ is replaced by $\ell'_{x,y}$. If $\Delta H > 0$, then generate a random number \mathcal{R} and compare to $e^{-\Delta H}$ to decide whether the height of membrane should be changed or not. We also choose periodic boundary condition in all our simulations.

3.1.3 Snapshots in MC Simulations

The parameters in the simulations are listed in Table. 3.1. Two snapshots of the contours of the membrane height with $E_{eff1} = E_{eff2} = 1$, $\Lambda_1 = \Lambda_2 = 0.2$, $\ell_1 = 15$, and $\ell_2 = 21$ (i.e., $g = 3.6$) are shown in Fig. 3.1 and Fig. 3.2. The parameters are chosen such that the system is in two phase region, far from critical region. In Fig. 3.1, the initial membrane height is set to be ℓ_1 , the natural length of type-1

Table 3.1: Parameters in simulations

<hr/>	
symbol	values
<hr/> <hr/>	
Γ	0.0025
Λ_1, Λ_2	0.2
ℓ_1	15
<hr/>	

junction. The height of the black patches is smaller than ℓ_1 , the height of the dark gray patches is in the interval between ℓ_1 and $\frac{1}{2}(\ell_1 + \ell_2)$. In Fig. 3.2, the initial membrane height is set to be ℓ_2 , the natural length of type-2 junction. The height of the light gray patches is in the interval between $\frac{1}{2}(\ell_1 + \ell_2)$ and ℓ_2 , the height of the white patches is larger than ℓ_2 . Both figures show that in two phase region, the equilibrium membrane height depends on the initial condition (i.e., the natural length of type- α junction). It is because the barrier height between the potential minimums is so large comparing to the thermal fluctuation. Thus, the distribution of the equilibrium membrane height is near the initial membrane height. Fig. 3.3 and Fig. 3.4 are snapshots for $E_{eff1} = E_{eff2} = 1$, $\Lambda_1 = \Lambda_2 = 0.2$, $\ell_1 = 15$, and $\ell_2 = 20$ ($g = 2.5$) on a 64×64 lattice. The set of parameters corresponds to a system near

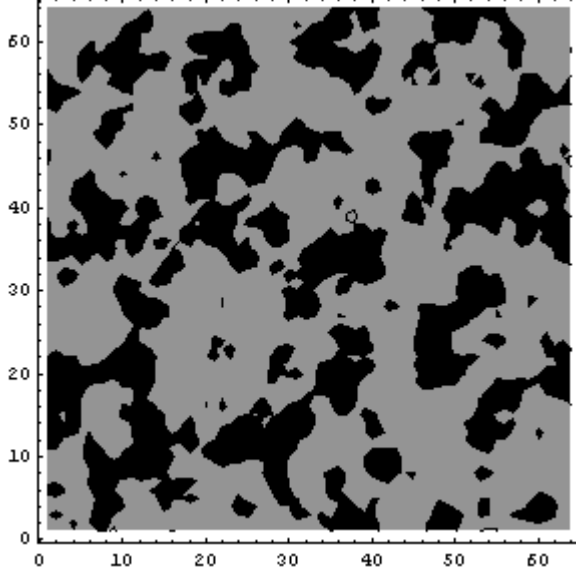


Figure 3.1: Snapshot of the contours of the membrane height with $E_{eff1} = E_{eff2} = 1$, $\Lambda_1 = \Lambda_2 = 0.2$, $\ell_1 = 15$, and $\ell_2 = 21$ ($g = 3.6$) on a 64×64 lattice. The parameters are chosen such that the system is in two phase region, far from critical region. The initial membrane height is set to be ℓ_1 , the natural length of type-1 junction. The height of the black patches is smaller than ℓ_1 , the height of the dark gray patches is in the interval between ℓ_1 and $\frac{1}{2}(\ell_1 + \ell_2)$. That is, in this region the equilibrium membrane height is near the natural length of type-1 junction, the initial membrane height.

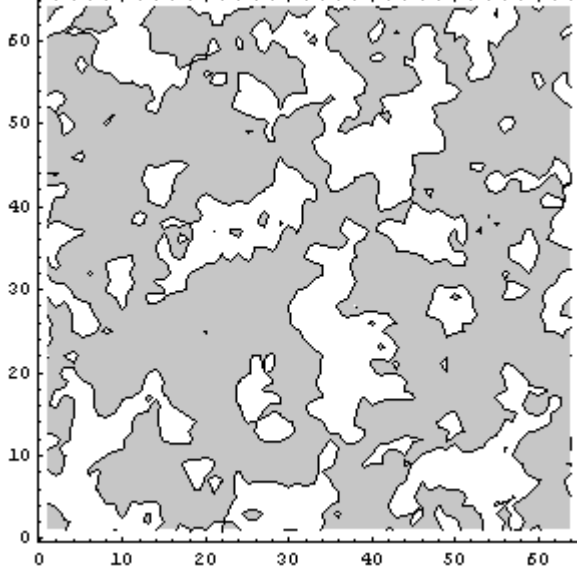


Figure 3.2: Snapshot of the contours of the membrane height with $E_{eff1} = E_{eff2} = 1$, $\Lambda_1 = \Lambda_2 = 0.2$, $\ell_1 = 15$, and $\ell_2 = 21$ ($g = 3.6$) on a 64×64 lattice. The parameters are chosen such that the system is in two phase region, far from critical region. The initial membrane height is set to be ℓ_2 , the natural length of type-2 junction. The height of the light gray patches is in the interval between $\frac{1}{2}(\ell_1 + \ell_2)$ and ℓ_2 , the height of the white patches is larger than ℓ_2 . That is, in this region the equilibrium membrane height is near the natural length of type-2 junction, the initial membrane height.

critical point. In Fig. 3.3, the initial membrane height is set to be ℓ_1 , the natural length of type-1 junction. In Fig. 3.4, the initial membrane height is set to be ℓ_2 , the natural length of type-2 junction. In both figures, the black, dark gray, light gray, and white color represent the membrane height ℓ correspond to $\ell < \ell_1$, $\ell_1 < \ell < \frac{1}{2}(\ell_1 + \ell_2)$, $\frac{1}{2}(\ell_1 + \ell_2) < \ell < \ell_2$, and $\ell > \ell_2$ respectively. In this region, the equilibrium membrane height is independent of the initial condition because the thermal fluctuations make the membrane height change from shorter (higher) junction phase to higher (shorter) junction phase. The above figures show the snapshots of the equilibrium membrane height for large g (far from the critical region) and small g (near the critical region). However, it is very difficult to locate the critical point by looking at the snapshots. Thus, we introduce a systematic method “Binder cumulant” to determine the critical points.

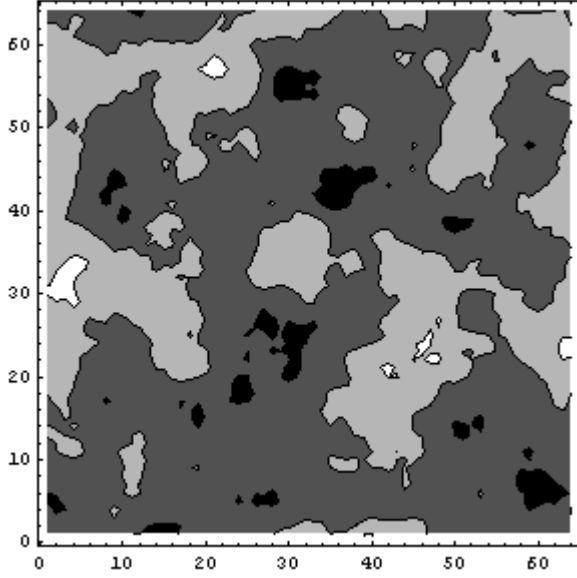


Figure 3.3: Snapshot of the contours of the membrane height with $E_{eff1} = E_{eff2} = 1$, $\Lambda_1 = \Lambda_2 = 0.2$, $\ell_1 = 15$, and $\ell_2 = 20$ ($g = 2.5$) on a 64×64 lattice. The parameters are chosen such that the system is in one phase region, near critical region. The initial membrane height is set to be ℓ_1 , the natural length of type-1 junction. The black, dark gray, light gray, and white color represent the membrane height ℓ correspond to $\ell < \ell_1$, $\ell_1 < \ell < \frac{1}{2}(\ell_1 + \ell_2)$, $\frac{1}{2}(\ell_1 + \ell_2) < \ell < \ell_2$, and $\ell > \ell_2$ respectively.

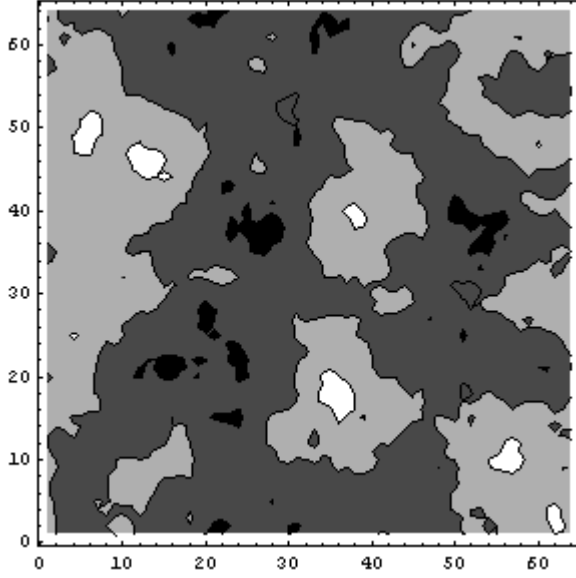


Figure 3.4: Snapshot of the contours of the membrane height with $E_{eff1} = E_{eff2} = 1$, $\Lambda_1 = \Lambda_2 = 0.2$, $\ell_1 = 15$, $\ell_2 = 20$ ($g = 2.5$) on a 64×64 lattice. The parameters are chosen such that the system is in one phase region, near critical region. The initial membrane height is set to be ℓ_2 , the natural length of type-2 junction. The black, dark gray, light gray, and white color represent the membrane height ℓ corresponds to $\ell < \ell_1$, $\ell_1 < \ell < \frac{1}{2}(\ell_1 + \ell_2)$, $\frac{1}{2}(\ell_1 + \ell_2) < \ell < \ell_2$, and $\ell > \ell_2$ respectively.

3.2 The Binder Cumulant and Critical Point

In last section, we have shown that it is difficult to determine the critical point quantitatively by looking at the snapshots of the simulations. Thus, we introduce the Binder cumulants C_2 and C_4 which are defined as [24]:

$$C_2 = \frac{\langle \bar{z}^2 \rangle}{\langle |\bar{z}| \rangle^2}, \quad C_4 = \frac{\langle \bar{z}^4 \rangle}{\langle \bar{z}^2 \rangle^2}, \quad (3.2)$$

where $\bar{z} = \frac{1}{N} \sum_{i=1}^N z_i$ is the spatial average of the order parameter, $z_i = \ell_i - \ell_0$, and $\langle \mathcal{O} \rangle$ is the thermal averages of \mathcal{O} . For $g > g_c$ (critical value of g) and $L \gg \xi$ (the correlation length of z), the Binder cumulants reach the values $C_2 = 1$ and $C_4 = 1$. For $0 < g < g_c$ and $L \gg \xi$, we have $C_2 = \pi/2 \approx 1.57$ and $C_4 = 3$. For $0 < g < g_c$ and $L \ll \xi$, the moments C_2 and C_4 vary only weakly with the linear size L . Therefore the critical value of g can be estimated from the common intersection of C_2 and C_4 , respectively, as a function of g for several values of L [23], [24].

3.3 Results and Discussions

The number of type- α junctions is determined by Eq.(2.7), and we rewrite it as

$$N_\alpha = \sum_i \left\langle \frac{e^{E_{eff\alpha} - \frac{1}{2}\Lambda_\alpha(\ell_i - \ell_\alpha)^2}}{1 + \sum_{\beta=1}^2 e^{E_{eff\beta} - \frac{1}{2}\Lambda_\beta(\ell_i - \ell_\beta)^2}} \right\rangle, \quad (3.3)$$

where ℓ_i is the membrane height at site i at some instance. Thus, we can calculate the density of type- α junction in the simulations. When the system reaches equilibrium, the dimensionless chemical potential (energy unit is chosen to be $k_B T$) of type- α junctions ($\tilde{\mu}_\alpha$), free ligands ($\tilde{\mu}_{L\alpha}$), and free receptors ($\tilde{\mu}_{R\alpha}$) satisfy the condition

$$\tilde{\mu}_\alpha = \tilde{\mu}_{R\alpha} + \tilde{\mu}_{L\alpha}. \quad (3.4)$$

The chemical potentials of the free ligands and receptors are related to their densities by $\psi_{L\alpha} = e^{\tilde{\mu}_{L\alpha}}$ and $\psi_{R\alpha} = e^{\tilde{\mu}_{R\alpha}}$, and we assume $\tilde{\mu}_{R\alpha} = \tilde{\mu}_{L\alpha}$. Therefore, the relations between E_{eff+} and total density of junctions and free ligands and receptors are shown in Tab. 3.2. It is clear that the density increase as the effective binding energy increases. For higher total effective binding energy (E_{eff+}), the total junction density is higher. It is because the effective binding energy is the sum of the binding energy and the entropy lost due to the formation of ligand-receptor pair (junction). For larger effective binding energy, the ligand and receptor prefer to bind to each other. In biological systems, typical values of the number of ligands ($N_{L\alpha}$) and receptors ($N_{R\alpha}$) are on the order 10^5 per cell, where the area of the cell (A_c) $\sim 10 - 10^4 \mu m^2$. In general case, we expect that total number of free type- α ligands and receptors are the same order as $N_{L\alpha}$ and $N_{R\alpha}$. Thus typical values of $\psi_{L\alpha}$ and $\psi_{R\alpha}$ should be $\mathcal{O}(10^{-2})$, and typical binding energy $E_{B\alpha} \sim 10-20 k_B T$, typical E_{eff1} and E_{eff2} should be of order unity, and they can be positive or negative. As shown in Tab. 3.2, our choice of parameters correspond to typical biological systems.

Typical C_2 (Fig. 3.5) and C_4 (Fig. 3.6) diagrams for several values of L are shown. From Fig. 3.5 and 3.6, we find that $g_c \simeq 2.8$. We can estimate critical point in this way for different E_{eff+} . Therefore, we plot the critical values of g with respect to E_{eff+} in Fig. 3.7. It shows that the critical value of g decreases with the increase of E_{eff+} , this is because the fluctuation of the membrane is smaller when the junction density is higher.

Table 3.2: Total density of junctions and free ligands and receptors

E_{eff+}	junctions(%)	free ligands and receptors(%)
<hr/>		
-8	~ 1.6	$\sim 2 \times 10^{-4}$
-6	~ 4.8	$\sim 5 \times 10^{-3}$
-4	~ 11.2	$\sim 10^{-3}$
-2	~ 28	$\sim 3 \times 10^{-3}$
0	~ 50	$\sim 9 \times 10^{-3}$
2	~ 73	~ 0.03
4	~ 87	~ 0.07
6	~ 95	~ 0.2
8	~ 98	~ 0.5

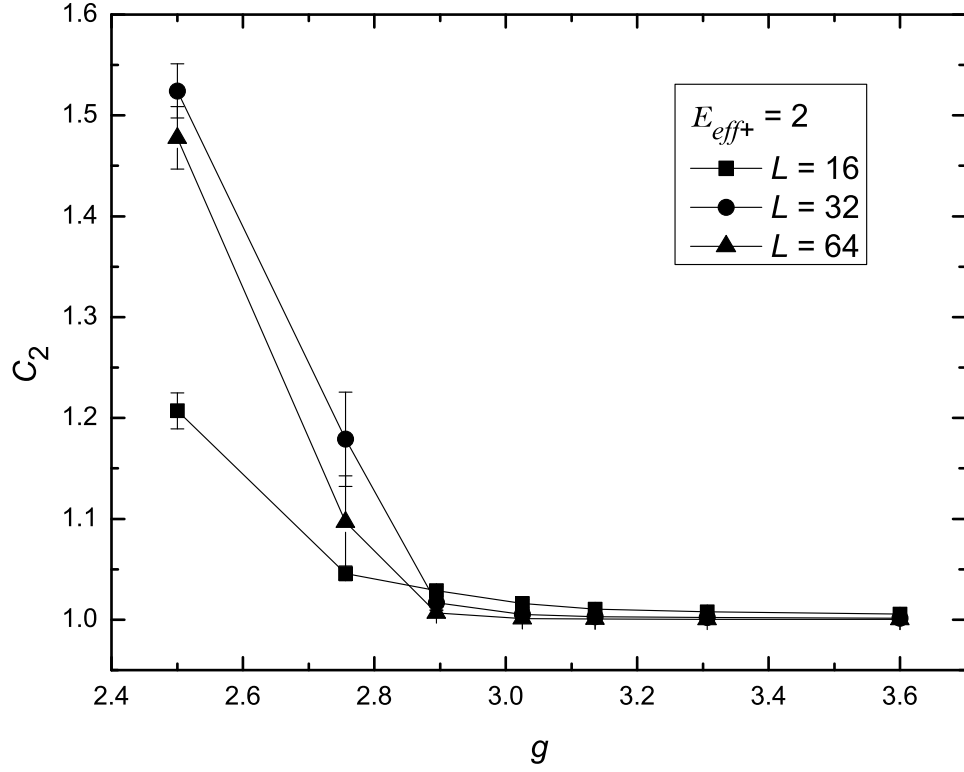


Figure 3.5: C_2 as a function of g for $L = 16$ (square), 32 (circle), and 64 (triangle) with parameters $\Lambda_1 = \Lambda_2 = 0.2$, $E_{eff+} = 2$ ($E_{eff1} = E_{eff2} = 1$), and $\ell_1 = 15$. The common intersection point in this case is near $g = 2.8$.

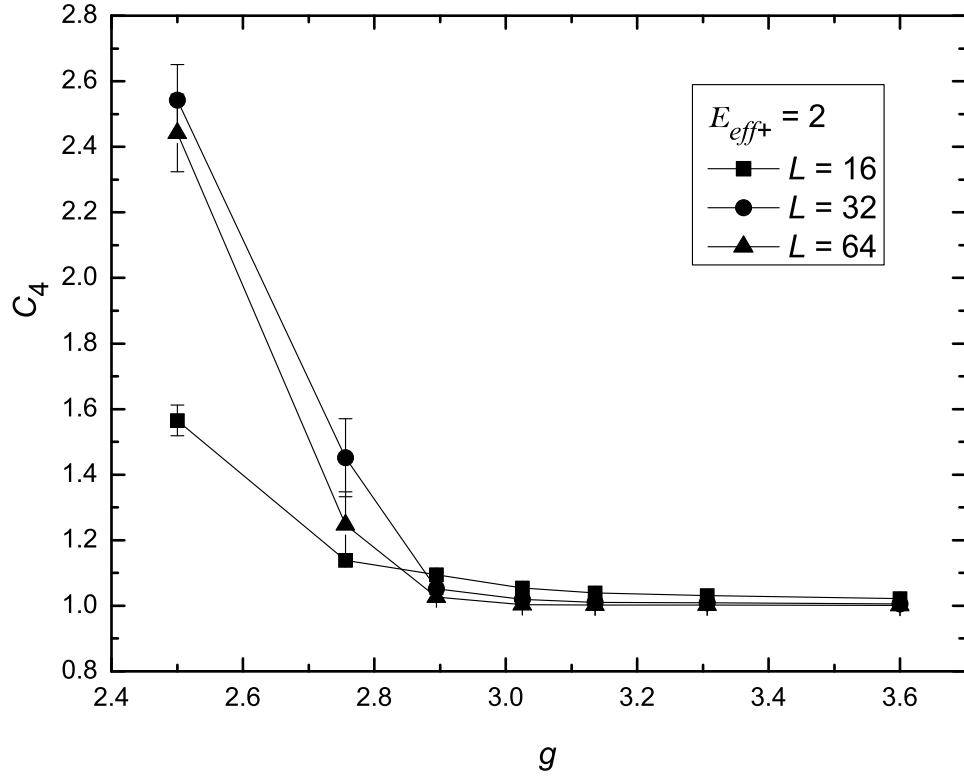


Figure 3.6: C_4 as a function of g for $L = 16$ (square), 32 (circle), and 64 (triangle) with parameters $\Lambda_1 = \Lambda_2 = 0.2$, $E_{eff+} = 2$ ($E_{eff1} = E_{eff2} = 1$), and $\ell_1 = 15$. The common intersection point in this case is near $g = 2.8$.

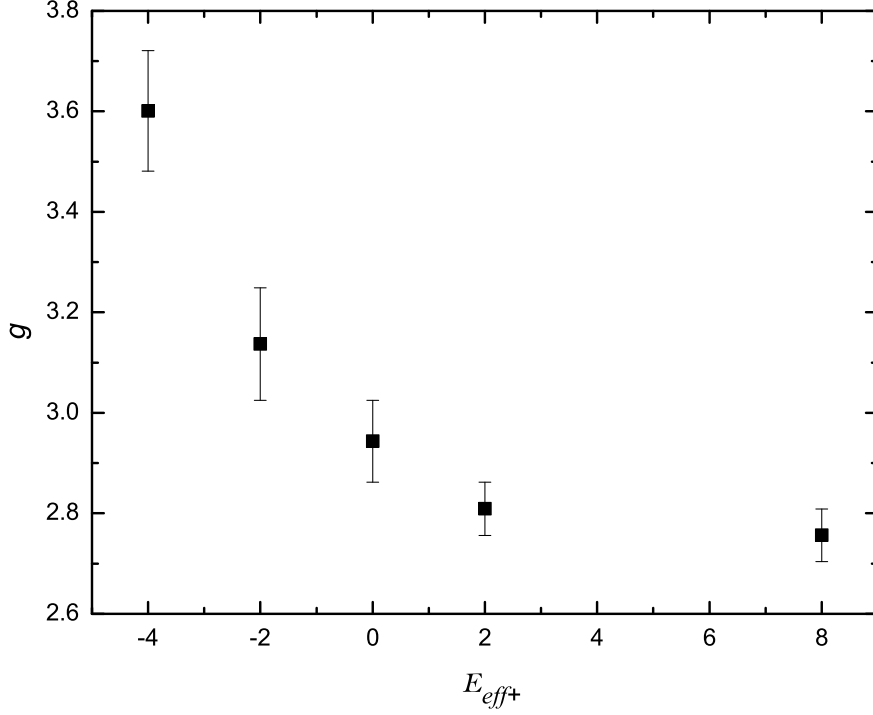


Figure 3.7: The critical value of g as a function of E_{eff+} for $E_{eff-} = 0$, $\Lambda_+ = 0.4$, $\lambda = 0$, and $\ell_1 = 15$. The critical value of g decreases with the increase of E_{eff+} , this is because the fluctuation of the membrane is smaller when the junction density is higher. The data points in the figure are partial result of our simulations. It is because the statistical error increases as the value of E_{eff+} decreases. Thus, we show the data points for $-4 \leq E_{eff+} \leq 8$.

Chapter 4

Conclusions

In this thesis, we have studied the adhesion-induced phase separation of multi-component membranes by theoretical and numerical methods. In this system, two different types of junctions (they are different in the natural length and the flexibility) mediate the membrane adhesion. The phase diagram for a system with $\lambda > 0$ is shown schematically in Fig. 4.1. Three methods are used to study the phase separation of this system.

1. In mean field theory, we integrate over all distributions of junctions in the partition function and obtain an effective membrane potential. The junction height difference and the junction flexibility difference are two important factors that affect the phase behavior. We discuss the phase diagrams in both symmetric case (both types of junctions have the same flexibility but different natural length) and asymmetric case (different type of junctions have different flexibilities and natural length). After analyzing the properties of the potential, we find that in symmetric case, the phase separation is driven by the height difference of the junctions. In the region of suffi-

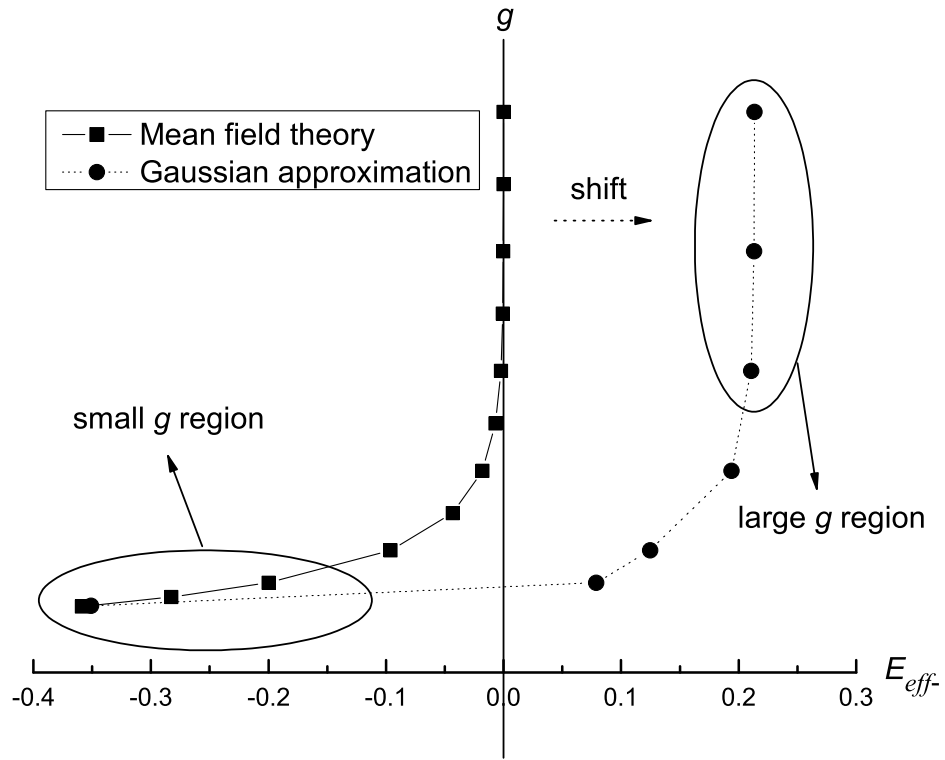


Figure 4.1: The schematic phase diagram for mean field theory (solid line) and Gaussian approximation (dashed line).

ciently large height difference in the asymmetric case, the junction height difference is the main factor that drives the phase separation. However, in the small height difference region in the asymmetric case, the minimum energy of the more rigid junctions is “lowered” by the binding energy of the softer junctions. As a result, in this region the phase coexistence occurs when the effective binding energy of the more rigid (softer) junctions are smaller (larger). Thus, the phase boundary moves toward smaller E_{eff-} .

2. Gaussian approximation is used to study the fluctuation effect on the phase coexistence curves of the asymmetric case. When the junction height difference is large, because the softer junctions can be stretched or compressed easier than the more rigid junctions and have higher entropy, comparing to the mean field theory, the phase coexistence curves move to higher effective binding energy of the more rigid junctions. Furthermore, the softer the junctions are, the higher the the entropy they have. Thus, the phase boundary shift is more significant for system with larger junction flexibility difference and smaller total junction effective binding energy. In small junction height difference region, the phase boundary moves toward the mean-field critical point as the junction height difference decreases (because Gaussian theory and mean field theory predict the same critical point).

3. Monte Carlo simulations simulate the symmetric case to study the effect of junction density on the critical point. We find that the junction density increases when the total effective binding energy increases. Meanwhile, the phase separation occurs at larger junction height difference when junction density of the system is lower. Because the fluctuation of membrane is smaller when the junction density is

higher.

Experimentally, the transition from shorter-junction-rich phase to longer-junction-rich phase can be induced by applying a mechanical pulling force on the system. This is because the effective binding energy of the longer junctions increases and that of the shorter junctions decrease under a pulling force. Thus, the phase transition can be observed in typical experiments.

In summary, we have provided a general physical picture for the adhesion-induced phase separation of multi-component membranes. In our theory, we assume that the membranes bind to each other in the whole process. It is possible to study binding/unbinding transition in the future. In this case, the membrane-membrane collisions may drive a different kind of phase separation. Another possible future work is to study the dynamics of adhesion and detachment of this type of systems.

APPENDICES

Appendix A

Elasticity of two fluctuating membranes

This appendix shows the calculation that reduces a two-membrane Hamiltonian to a single-membrane Hamiltonian. If we consider only the bending energy of the membranes then the Hamiltonian of the system with two membranes in the solvent can be written as

$$H = \int d^2r \left\{ \frac{\kappa_1}{2} [\nabla^2 z_1(\mathbf{r})]^2 + \frac{\kappa_2}{2} [\nabla^2 z_2(\mathbf{r})]^2 \right\}, \quad (\text{A.1})$$

where z_1 and z_2 are the height of the upper membrane and the lower membrane from the reference plane, respectively. Define $u = z_1 + z_2$ and $h = z_1 - z_2$, thus $z_1 = \frac{1}{2}(u + h)$ and $z_2 = \frac{1}{2}(u - h)$. Substitute $[\nabla^2 z_1]^2 = [\frac{1}{2}(\nabla^2 u + \nabla^2 h)]^2$ and $[\nabla^2 z_2]^2 = [\frac{1}{2}(\nabla^2 u - \nabla^2 h)]^2$ into Eq. (A.1) leads to

$$\begin{aligned} H = & \frac{1}{8} \int d^2r \left\{ (\kappa_1 + \kappa_2) [\nabla^2 u(\mathbf{r})]^2 + (\kappa_1 + \kappa_2) [\nabla^2 h(\mathbf{r})]^2 \right. \\ & \left. + 2(\kappa_1 - \kappa_2) \nabla^2 u(\mathbf{r}) \nabla^2 h(\mathbf{r}) \right\} \end{aligned}$$

$$\begin{aligned}
= & \int d^2r \left\{ \frac{1}{2} \frac{\kappa_1 \kappa_2}{\kappa_1 + \kappa_2} [\nabla^2 h(\mathbf{r})]^2 + \frac{\kappa_1 + \kappa_2}{8} [\nabla^2 u(\mathbf{r}) \right. \\
& \left. + \frac{\kappa_1 - \kappa_2}{\kappa_1 + \kappa_2} \nabla^2 h(\mathbf{r})]^2 \right\} \tag{A.2}
\end{aligned}$$

We integrate out the second term in Eq. (A.2) and define $\kappa = \frac{\kappa_1 \kappa_2}{\kappa_1 + \kappa_2}$, then the Hamiltonian becomes

$$H = \int d^2r \left\{ \frac{\kappa}{2} [\nabla^2 h(\mathbf{r})]^2 \right\}. \tag{A.3}$$

Similarly, for systems with non-vanishing surface tension,

$$H = \int d^2r \left\{ \frac{\kappa}{2} [\nabla^2 h(\mathbf{r})]^2 + \frac{\gamma}{2} [\nabla h(\mathbf{r})]^2 \right\}, \tag{A.4}$$

where $\gamma = \frac{\gamma_1 \gamma_2}{\gamma_1 + \gamma_2}$.

Appendix B

Nondimensionalization of the Hamiltonian

The Hamiltonian of the system is

$$\begin{aligned}
 H = \int dx dy \left\{ \frac{\kappa}{2} [\nabla^2 h(x, y)]^2 + \frac{\gamma}{2} [\nabla h(x, y)]^2 \right. \\
 \left. + \sum_{\alpha=1}^2 \Phi_{\alpha}(x, y) \frac{\lambda_{\alpha}}{2} [h(x, y) - h_{\alpha}]^2 - \sum_{\alpha=1}^2 \Phi_{\alpha} E_{B\alpha} \right\}. \quad (\text{B.1})
 \end{aligned}$$

The unit length in z -direction is $h_0 = a/\sqrt{\frac{\kappa}{k_B T}}$. The discretized Laplacian and gradient of h in two dimensional space are

$$\begin{aligned}
 \nabla^2 h &= \frac{\partial^2 h}{\partial x^2} + \frac{\partial^2 h}{\partial y^2} \\
 &= \frac{\partial}{\partial x} \left(\frac{h_{x+\frac{a}{2},y} - h_{x-\frac{a}{2},y}}{a} \right) + \frac{\partial}{\partial y} \left(\frac{h_{x,y+\frac{a}{2}} - h_{x,y-\frac{a}{2}}}{a} \right) \\
 &= \frac{1}{a^2} (h_{x+a,y} + h_{x-a,y} + h_{x,y+a} + h_{x,y-a} - 4h_{x,y}) \\
 &= \frac{1}{a} \sqrt{\frac{k_B T}{\kappa}} (\ell_{x+a,y} + \ell_{x-a,y} + \ell_{x,y+a} + \ell_{x,y-a} - 4\ell_{x,y}) \\
 &\equiv \frac{1}{a} \sqrt{\frac{k_B T}{\kappa}} \Delta_d \ell_{x,y} = \frac{1}{a} \sqrt{\frac{k_B T}{\kappa}} \Delta_d \ell_i \quad (\text{B.2})
 \end{aligned}$$

and

$$\begin{aligned}
\nabla h &= \frac{\partial h}{\partial x} \hat{\mathbf{i}} + \frac{\partial h}{\partial y} \hat{\mathbf{j}} \\
&= \frac{1}{2a} \left[(h_{x+a,y} - h_{x-a,y}) \hat{\mathbf{i}} + (h_{x,y+a} - h_{x,y-a}) \hat{\mathbf{j}} \right] \\
&= \frac{1}{2a} \sqrt{\frac{k_B T}{\kappa}} [(\ell_{x+a,y} - \ell_{x-a,y}) \hat{\mathbf{x}} + (\ell_{x,y+a} - \ell_{x,y-a}) \hat{\mathbf{y}}] \\
&\equiv \frac{1}{2a} \sqrt{\frac{k_B T}{\kappa}} \nabla \ell_{x,y} = \frac{1}{2a} \sqrt{\frac{k_B T}{\kappa}} \nabla \ell_i.
\end{aligned} \tag{B.3}$$

Also defined here is $\phi_\alpha(x, y) = a^2 \Phi_\alpha(\mathbf{r})$, the number of type- α junctions at site (x, y) .

Hence, the non-dimensionalized Hamiltonian of the system is

$$\begin{aligned}
\tilde{H} &= \sum_{i=1}^N \left\{ \frac{1}{2} (\Delta_d \ell_i)^2 + \frac{1}{2} \frac{\gamma a^2}{\kappa} (\nabla \ell_i)^2 \right. \\
&\quad \left. + \sum_{\alpha=1}^2 \phi_\alpha(i) \left[\frac{1}{2} \frac{\lambda_\alpha a^2}{\kappa} [\ell(i) - \ell_\alpha]^2 - \tilde{E}_{B\alpha} \right] \right\}.
\end{aligned} \tag{B.4}$$

BIBLIOGRAPHY

Bibliography

- [1] R. Bruinsma, M. Goulian, and P. Pincus, *Biophys. J.* **67**, 746, (1994).
- [2] D. Zuckerman and R. Bruinsma, *Phys. Rev. Lett.*, **74**, 3900, (1995).
- [3] R. Lipowsky and E. Sackmann, *The Structure and Dynamics of Membranes*, (Elsevier, Amsterdam, 1995).
- [4] R. Lipowsky, *Phys. Rev. Lett.*, **77**, 1652, (1996).
- [5] A. Albersdörfer, T. Feder, and E. Sackmann, *Biophys. J.*, **73**, 245, (1997).
- [6] J. Nardi, T. Feder, and E. Sackmann, *Europhys. Lett.* **37**, 371, (1997).
- [7] R. Bruinsma, A. Behrisch, and E. Sackmann, *Phys. Rev. E*, **61**, 4253, (2000).
- [8] T. R. Weigl, R. R. Netz, and R. Lipowsky, *Phys. Rev. E*, **62** R45, (2000).
- [9] S. Komura and D. Andelman, *Eur. Phys. J. E*, **3** 259, (2000).
- [10] T. R. Weigl and R. Lipowsky, *Phys. Rev. E*, **64**, 011903, (2001).
- [11] N.J. Burroughs and C. Wülfing, *Biophys. J.* **83**, 1784, (2002).

- [12] C. R. F. Monks, et. al., Nature, **395**, 82, (1998), G. Grakoui, et. al., Science, **285**, 221, (1999), and D. M. Davis, et. al., Proc. Natl. Acad. Sci. USA, **96**, 15062, (1999).
- [13] B. Alberts, D. Bray, J. Lewis, M. Faff, K. Roberts, and J. D. Watson, *Molecular Biology of the Cell*, 3rd ed. (Garland, New York, 1994).
- [14] See, S.Y. Qi, J. T. Groves, and A. K. Chakraborty, Proc. Natl. Acad. Sci. USA, **98**, 6548, (2001).
- [15] S. Raychaudhuri, A. K. Chakraborty, and M. Kardar, Phys. Rev. Lett. **91**, 208101, (2003).
- [16] T.R. Weikl, J.T. Groves, and R. Lipowsky, Europhys. Lett. **59**, 916 (2002).
- [17] T.R. Weikl and R. Lipowsky, Biophys. J. **87**, 3665, (2004).
- [18] H. Y. Chen, Phys. Rev. E, **67**, 031919,(2003).
- [19] H. Strey, M. Peterson, and E. Sackmann, Biophys. J. **69**, 478, (1995).
- [20] Needham. D. and R. M. Hochmuth, Biophys. J. **61**, 1664, (1992).
- [21] G.I. Bell, M. Dembo, and P. Bongrand, Biophys. J. **45**, 1051, (1984).
- [22] R. Geotz, G. Gompper, and R. Lipowsky, Phys. Rev. Lett., **82**, 221, (1999).
- [23] K. Binder and D. W. Heerman, *Monte Carlo Simulation in Statistical Physics An Introduction*, 2nd corrected ed. (Berlin, New York, Springer-Verlag, 1992).

- [24] T.R. Weigl, D. Andelman, S. Komura, and R. Lipowsky, Eur. Phys. J. E, **8**, 59, (2002).